Hindawi
International Journal of Photoenergy
Volume 2021, Article ID 9926316, 14 pages
https://doi.org/10.1155/2021/9926316

Research Article

On the Reliability of Transformerless Photovoltaic DC/AC Converters Based on Mission Profile

Ignacio Villanueva,[1] **Nimrod Vazquez**,[1] **Joaquín Vaquero**,[2] **Claudia Hernández**,[1] **Héctor López**,[1] **Rene Osorio**,[3] **and Sergio Pinto**[4]

[1]*Electronics Engineering Department, TecNM-Instituto Tecnológico de Celaya, 38010 Celaya, Mexico*
[2]*Electronics Technology Area, Rey Juan Carlos University, 28933 Mostoles, Madrid, Spain*
[3]*Computer Science and Engineering Department, University of Guadalajara, 46600 Ameca, Jalisco, Mexico*
[4]*Research Development and Innovation Department, International Maritime University of Panama and "Universidad de Panama", WCWQ+53 Panama, Panama*

Correspondence should be addressed to Nimrod Vazquez; n.vazquez@ieee.org

Received 28 May 2021; Revised 29 July 2021; Accepted 19 August 2021; Published 11 November 2021

Academic Editor: Sergiu Spataru

Photovoltaic systems are a technology for the generation of electrical energy that is constantly increasing thanks to current technological advances and that contributes to sustainable development. The main stages of photovoltaic systems are the conversion stage, using an inverter, and filtering. These systems may be considered as a mature and growing technology; however, regarding its reliability, there exists some uncertainties, and they are related to the operation, incidents, and its potential failures, due to the number of elements, the environment, and the operating nominal values. For this reason, this article presents a comparative analysis of the reliability of single-phase transformerless photovoltaic inverters used to inject active power into the grid. This evaluation is carried out under the same design specifications for all the inverters analyzed; the study is made using a mission profile considering the IEC TR 62380 standard, where the events and environmental operating conditions are defined, and numerical simulations. This work is aimed at providing suggestions to improve the quality of the photovoltaic system also considering reliability.

1. Introduction

Energy is an essential part of the technological and economic development of countries and regions worldwide. The constant increment in the demand and price of energy in industrialized countries has gradually led to the substitution of fossil fuels for the use of alternative energies. The higher use of those energies, mainly wind and solar photovoltaic, brings favorable effects on the environment, such as the reduction of greenhouse gases and other types of pollutants [1–4].

The great number of advantages that this type of energy presents is remarkable. However, the way in which energy is produced has certain technical disadvantages, such as dependent on climatic conditions, which implies a deficiency in energy production [3–5].

Nowadays, environmentally friendly energies have been developed but with some drawbacks such as high penetration, which causes certain problems within the electrical grid, such as voltage variations. The control of those systems is very complex; therefore, the useful life and reliability of photovoltaic systems are becoming important factors [5–7].

Advances in power electronics have allowed the application of transformerless inverters, used in photovoltaic systems. They have good efficiency, low volume, and lightweight. These topologies are operated to not generate a common-mode voltage in order to avoid the generation of leakage currents between the photovoltaic module and the ground. The evolution of these systems brings with it the optimization and improvement of the semiconductors that make up the system, such as higher voltages and

nominal powers, best efficiencies, higher thermal resistance, higher reliability, and lower cost [5–8].

The reliability of semiconductors and capacitors is affected by operating temperature. Therefore, the system losses could lead to a failure in the semiconductor devices, such as MOSFETs and filter capacitors. The set of operating environmental conditions of a system during its useful life is called the mission profile. It is very important to design a real field mission profile, under which the system will be operating. In this way, its reliability and service life can be guaranteed; that is, the system should be designed for an environment with conditions similar to those that would be operating normally [9, 10].

The most recent studies of reliability prediction are based on the design of the mission profile, where the phases, events, and operating environments define the mission [10, 11]. In [12], the authors calculate the converter reliability using different prototypes and semiconductors by using the IEC TR 62380 standard, taking into account an annual mission profile and the effect of extreme thermal cycles in a desert area. The authors of [13] present tools for the design of the safe operation mission profile for photovoltaic inverters connected to the grid with LCL filter, based on silicon carbide devices, including electrothermal models to predict junction temperature of the device case. In [14], it is evaluated the reliability of three transformerless inverters under an annual mission profile, taking into account the thermal load of the device, which is used for the prediction of the useful life, providing new ways for the design of photovoltaic systems.

In this paper, the reliability analysis of different single-phase transformerless photovoltaic inverters is made, including an LCL filter. In each inverter, the reliability prediction is calculated using the model of French Telecommunications standard IEC TR 62380. The study considers simulations using the PSIM software for the different transformerless LCL inverter topologies. The objective is to determine what single-phase inverter topology presents the best reliability, based on the effects of the mission profile during a period. A discussion is presented on which topology is recommended based on its longevity, and comments are provided on the factors that influence failure rates, how to improve efficiency, reliability, and useful life of the photovoltaic system.

The article is organized as follows: A background on transformerless photovoltaic inverters is presented, the IEC TR 62380 reliability standard is described, and the design and simulations are shown. Subsequently, a quantitative analysis of the reliability employing the standard is determined, the results are also analyzed, and finally, some conclusions are presented.

2. Photovoltaic Inverters and Reliability

In this section, the single-phase photovoltaic inverters, the mission profile, and the IEC TR 62380 standard are addressed to provide the basis for the employed PV converters and reliability analysis considering the mission profile.

2.1. Photovoltaic Inverters. The single-phase inverters used for active power injection may use a transformer, which allows to protect and avoid leakage currents between the photovoltaic system to the ground [15]. The advantage of connecting the inverter with a low-frequency transformer is galvanic isolation between the input and the output, but it has disadvantages such as its low efficiency and big size [5]. Another part of the system is the passive elements of the output filter. The most common configurations are L, LC, and LCL filters; the latter being the one that has the advantage of smallest size and highest efficiency.

To increase the efficiency and reduce the volume, a transformerless topology may be employed; however, a high leakage current may appear [16, 17]. There are different strategies to reduce the leakage current in transformerless photovoltaic inverters connected to the electrical grid.

One strategy is to use a modulation technique that does not generate common-mode voltage variations.

The full-bridge inverter (Figure 1) is one of the simplest inverters. Consists of four switches organized in two legs, the first formed by S_1 and S_2 and the second by S_3 and S_4. This configuration has four switching states and three different output voltage levels. Two PWM modulation schemes may be employed: bipolar and unipolar modulations [6, 15, 16, 18] and [19]. The unipolar modulation is not good to avoid common-mode voltage, and the bipolar modulation should be preferred. However, in this case, a disdvantage is the incresed size of the output filter.

The dual buck inverter (Figure 2), based on the full-bridge topology, combines two unidirectional buck converters during the positive half cycle, S_1 switching at high frequency, while S_4 is always on. During the negative half-cycle, S_2 switches at high frequency, while S_3 is always on. This produces a unipolar modulation. According to the literature, one of the advantages is the high reliability; due to the diodes connected in series to the inductor, there are no tripping problems and reverse recovery issues [4, 15], and [20].

Another technique used to reduce the leakage current is the disconnection of the photovoltaic module but keeping the unipolar modulation. In this case, switches are added on the DC or AC side of the inverter to disconnect the photovoltaic module from the grid and to create new routes to reduce the leakage current.

H5 topology (Figure 3) is based on the full-bridge topology; a switch is added on the DC side. The operation is similar to that of the full-bridge inverter, but adding switch S_5, its main function is to decouple the DC side from the AC side. Switches S_1 and S_3 commute at grid frequency, switch S_2 switches only in the negative half cycle, and switch S_4 only switches in the positive half cycle. Unipolar modulation is obtained and allows to reduce the leakage current [15, 18], and [19].

The HERIC topology (Figure 4) is derived from the full-bridge converter; however, a branch is added on the AC side in parallel to the bridge output, to isolate the PV panel from the grid. The switches S_1, S_2, S_3, and S_4 switch at high frequency; normally MOSFETs are used and S_5 and S_6 at grid frequency; regularly IGBT's are used. It integrates the

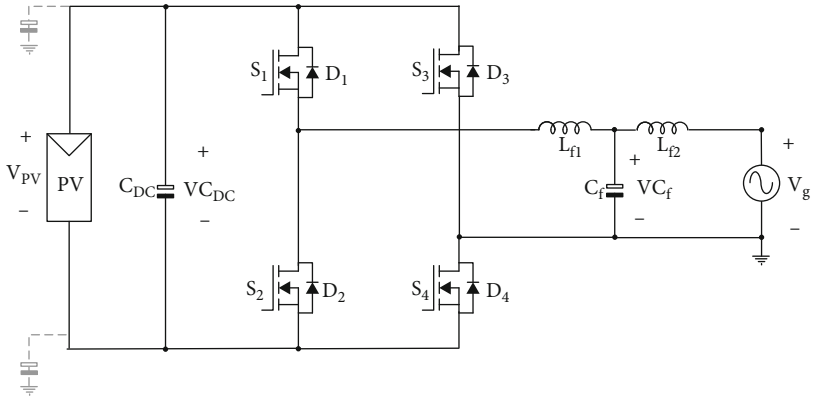

Figure 1: Full-bridge inverter.

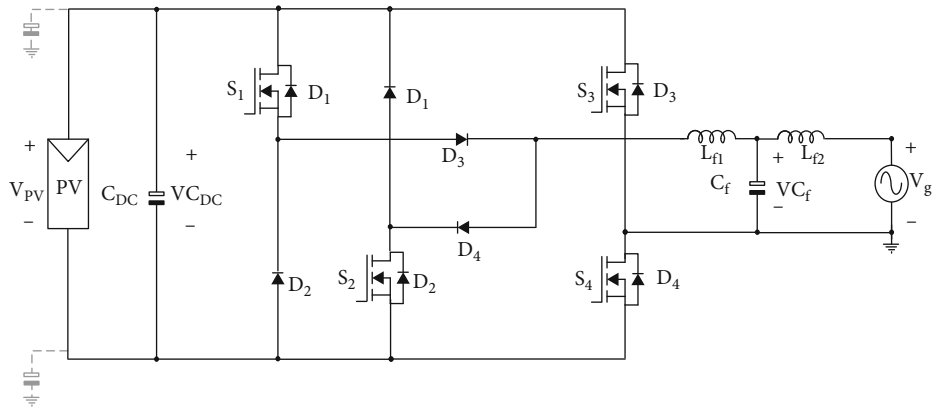

Figure 2: Dual buck inverter.

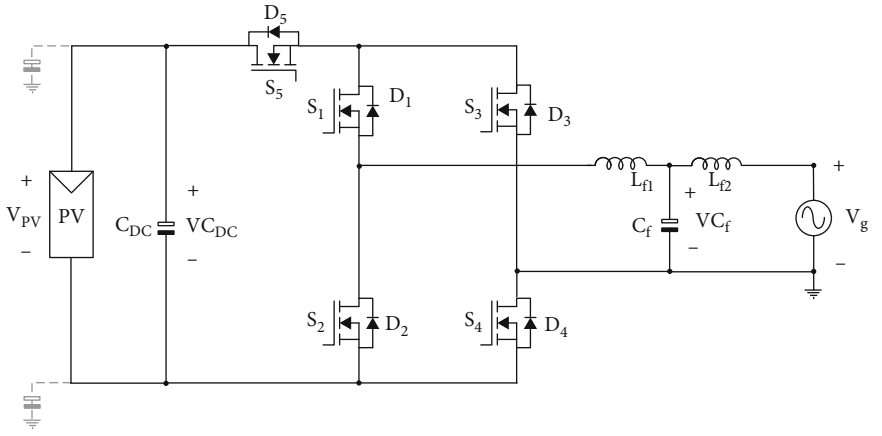

Figure 3: H5 inverter.

advantages of unipolar PWM modulation and reduces the leakage current of the solar panel [15, 18], and [19].

The H6 configuration (Figure 5) is based on the traditional full bridge as well, adding two switches and two diodes. For the operation, a unipolar modulation is considered, where the switches S_1, S_2, S_5, and S_6 are switched at high frequency and MOSFETs are regularly used. Switches S_3 and S_4 switch at grid frequency; IGBTs are generally used and provide a current path with diodes D_1 and D_2. During the free conduction time, during the positive half cycle, the current flows through S_4 and the diode D_1 allowing the disconnection between the photovoltaic module and the grid [4, 15], and [18].

Another alternative to reduce the leakage current is connecting the grid neutral point to the average input voltage, which eliminates variations in high frequency. The

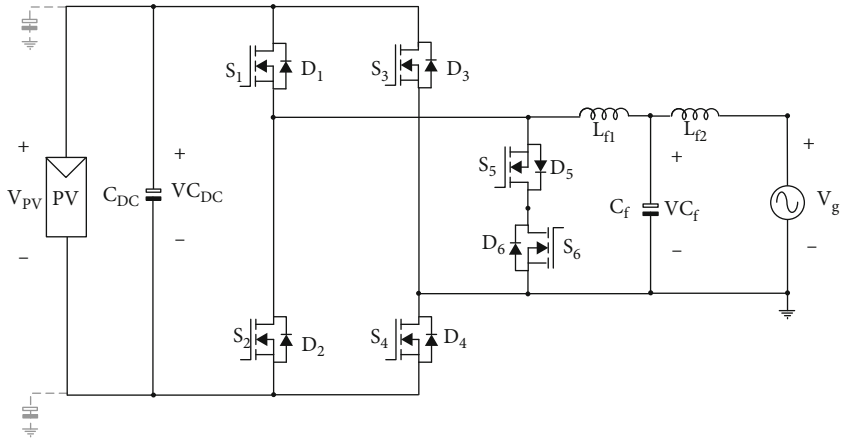

Figure 4: HERIC inverter.

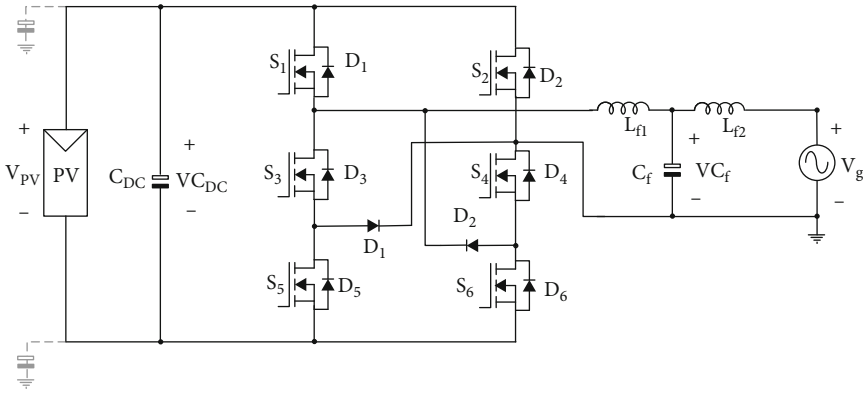

Figure 5: H6 inverter.

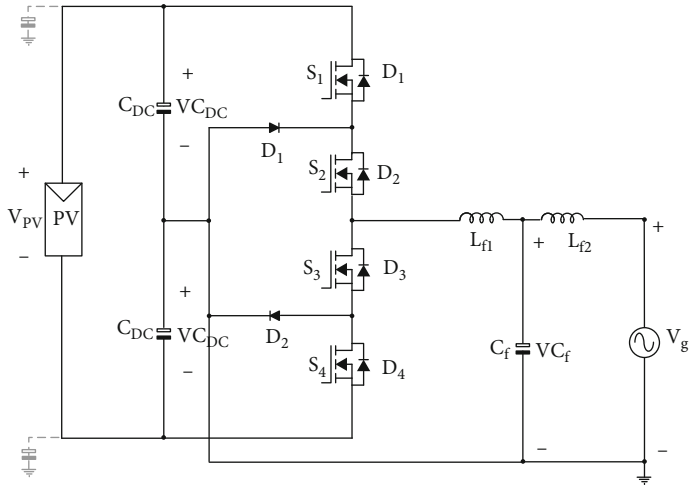

Figure 6: NPC inverter.

Neutral-Point Clamped (NPC) inverter fits in this category (Figure 6). It is composed of four switches; since two switches are added to the half-bridge inverter, the DC terminals are connected to two capacitors in series, which divide the panel voltage, providing a common or neutral point. The topology has two diodes connected to the neutral point. A unipolar modulation is used, and the output voltage has three levels [4, 6, 18], and [19].

Instead of connecting the grid neutral point to the average input voltage, the connection to the negative terminal of the PV panel can be made. The virtual DC bus topology considers this strategy (Figure 7); it is derived from the full-

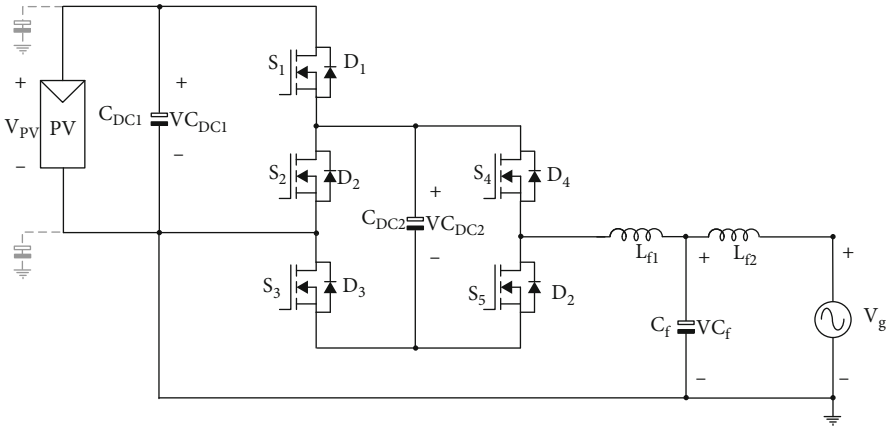

Figure 7: Virtual DC bus inverter.

bridge topology and consists of five switches S_1-S_5. The photovoltaic panel and capacitor C_{DC1} form a real DC bus; the virtual DC bus is generated by C_{DC2}. Capacitor C_{DC2} is charged through S_1 and S_3 to maintain a constant DC voltage. It can be controlled with a unipolar modulation [4, 15], and [21].

2.2. Mission Profile. A mission profile refers to define or represent certain characteristics or conditions of an operating environment. The mission profile is defined to reproduce the operating conditions of an electronic component set that represents the system to evaluate. That is, the environment, events, or phases of operation are defined (solar irradiance, temperature, operating time, among others), to which the components are subject during their life cycle and allows to evaluate reliability [9, 10].

Reliability is the probability that a component will function properly during the period for which it was designed, under the specific operating conditions. The mission profile must be clearly defined, to avoid inaccuracies in the reliability calculation, which will cause errors in the final development of the system [15].

The cases that are commonly used to define a mission profile based on a one-year cycle use component normal operation, like:

(a) On/off working phases with average outside temperatures

(b) Storage mode or inactive phases

(c) Permanent working phases with fluctuations in the average outside temperature

The mission profile parameters are defined as follows. The total annual relationship of times must be defined, in the printed circuit board (PCB) which will be in permanent operation mode (energized). This is represented by τ_{on} as:

$$\tau_{on} = \sum_{i=1}^{y} \tau_i, \tag{1}$$

where τ_i is the total annual relation of times for the PCB, in permanent operation mode, with supply and at the external ambient temperature (t_{ac}) that surrounds the equipment during the ith phase of the mission profile $(t_{ac})_i$.

It is also important to define the total annual relationship of times for the PCB in storage or inactive mode of operation. This is represented by τ_{off}:

$$\tau_{off} = 1 - \tau_{on}. \tag{2}$$

Adding τ_{on} in both terms of (2) is obtained:

$$\tau_{on} + \tau_{off} = 1. \tag{3}$$

The other parameter of the mission profile that is defined is the internal temperature increase in the components of the PCB compared to (t_{ac}) during the τ_{on} phase, and it is represented by $\Delta\tau_i$:

$$\Delta\tau_i = \left[\frac{\Delta T_j}{3} + (t_{ac})_i\right] - (t_{ae})_i, \tag{4}$$

where $(t_{ac})_i$ is the average ambient temperature of the PCB, close to the components (it is considered the most critical temperature), n_i represents the annual number of thermal cycles seen by the components of the PCB in phase ith of the mission profile with a temperature variation, and $\Delta\tau_i$ is defined as the average oscillations of the variation seen by the components of the PCB in the phase of the mission profile ith [11–14, 21].

2.3. Standard IEC TR 62380 and Reliability Design. There are different standards used for reliability prediction based on the mission profile. One of the best used is the IEC TR 62380 standard, which is a French standard (Union Technique de L'Électricité, UTEC C 80-810), which is used for the prediction of the reliability of electronic components, PCBs, and equipment.

In this standard, environmental factors are defined in the mission profile; the data contained in the standard is obtained from field data in different operating environments.

The reliability model used by the IEC TR 62380 standard is based on a failure rate model to be adjusted for each component defined as $\lambda_{\text{component}}$:

$$\lambda_{\text{component}} = \lambda_{\text{die}} + \lambda_{\text{package}}, \quad (5)$$

$$\lambda_{\text{die}} = \lambda_{\text{thermaleffects}} + \lambda_{\text{EOSeffects}}, \quad (6)$$

where λ_{die} is the failure rate related to the effects in operation, $\lambda_{\text{thermal effects}}$ is the failure rate related to thermal effects, $\lambda_{\text{EOS ffects}}$ is the failure rate related to the effects of electrical overstress, and λ_{package} is the failure rate related to thermo-mechanical effects.

Then, the model of the IEC TR 62380 standard is centered on the elements. In photovoltaic inverters, the main devices are the diode, the MOSFET, the capacitor, and the inductor.

The general mathematical model for the fit failure rate obtained by combining (5) and (6) is

$$\lambda_{\text{component}} = \lambda_{\text{thermal effects}} + \lambda_{\text{EOS effects}} + \lambda_{\text{package}}. \quad (7)$$

The general model (7) is used to adjust the failure rate of the components. Table 1 shows the factors and failure rates of adjustments from the general model, corresponding to the diode. The adjustment of the failure rate and factors of the MOSFET are shown in Table 2. The inductor failure rates are shown in Table 3. Finally, the failure rates of thermal and mechanical adjustments for the capacitor are shown in Table 4.

The parameters of Tables 1–4 are defined as follows:

λ_0 is the base failure rate given in the standard

λ_B is the base failure rate of the component packaging

λ_{EOS} is the failure rate related to electrical overstress in the application considered

π_U is the use factor for the diode (permanent or not); in switching conditions, it is considered permanent work

$(\pi_t)_i = i$th is the temperature factor related to the junction temperature T_j

$\tau_i = i$th is the component working time ratio to the junction temperature ith of the mission profile

$(\pi_n)_i = i$th is the influence factor related to the number of annual cycles of thermal variations observed in the packaging with amplitude $\Delta\tau_i$

$(\Delta\tau_i) = i$th is the variation of the temperature amplitude of the mission profile

π_1 is the influence factor related to the use of the component (protection interface or not)

π_S is the load factor for transistors related to the influence of the applied voltage

The π_S load factor described previously is used in the standard for power transistors (FET, MOS, and IGBT), which is given by:

$$\pi_S = \pi_{S1} + \pi_{S2}, \quad (8)$$

where $\pi_{S1} = 0.22e^{1.7S1}$ and $\pi_{S2} = 0.22e^{3S2}$.

Table 1: Adjustment failure rates for the diode.

	λ_{diode}
$\lambda_{\text{thermal effects}}$	$\{\pi_U.\lambda_0\}.\left\{\sum_{i=1}^{y}(\pi_t)_i.\tau_i/(\tau_{\text{on}}+\tau_{\text{off}})\right\}$
$\lambda_{\text{EOS effects}}$	$\left\{\left(2.75E^{-3}.\sum_{i=1}^{z}(\pi_n)_i.(\Delta T_i)^{0.68}\right).\lambda_B\right\}$
λ_{package}	$\{\pi_1.\lambda_B\}$

Table 2: Adjustment failure rates for the MOSFET.

	λ_{MOSFET}
$\lambda_{\text{thermal effects}}$	$\{\pi_S.\lambda_0\}.\left\{\sum_{i=1}^{y}(\pi_t)_i.\tau_i/(\tau_{\text{on}}+\tau_{\text{off}})\right\}$
$\lambda_{\text{EOS effects}}$	$\left\{\left(2.75E^{-3}.\sum_{i=1}^{z}(\pi_n)_i.(\Delta T_i)^{0.68}\right).\lambda_B\right\}$
λ_{package}	$\{\pi_1.\lambda_B\}$

Table 3: Adjustment failure rates for the inductor.

	$\lambda_{\text{inductor}}$
$\lambda_{\text{thermal effects}}$	$\lambda_0.\left\{\sum_{i=1}^{y}(\pi_t)_i.\tau_i/(\tau_{\text{on}}+\tau_{\text{off}})\right\}$
$\lambda_{\text{EOS effects}}$	$7E^{-3}.\left[\sum_{i=1}^{j}(\pi_n)_i.(\Delta T_i)^{0.68}\right]$

Table 4: Adjustment failure rates for the capacitor.

	$\lambda_{\text{capacitor}}$
$\lambda_{\text{thermaleffects}}$	$0.1.\left\{\sum_{i=1}^{y}(\pi_t)_i.\tau_i/(\tau_{\text{on}}+\tau_{\text{off}})\right\}$
$\lambda_{\text{EOSeffects}}$	$1.4E^{-3}.\left[\sum_{i=1}^{j}(\pi_n)_i.(\Delta T_i)^{0.68}\right]$

S_1 represents the quotient between the maximum applied repetitive voltage value and the specific nominal voltage in V_{DS}. S_2 is the quotient between the maximum applied repetitive voltage value and the specific nominal voltage in V_{GS}. They are determined by:

$$S_{1,2} = \frac{\text{Maximun repetitive voltage } V_{\text{DS}}, V_{\text{GS}}}{\text{Specific nominal voltage } V_{\text{DS}}, V_{\text{GS}}}. \quad (9)$$

The influence factor π_n depends on the number of annual cycles of thermal variations to which the component is subjected. There are two important relationships to define this parameter, which are shown below.

(a) If the component is subjected to $n \leq 8760$ thermal cycles/year, then $(\pi_n)_i = n_i^{0.76}$

(b) If the component is subjected to $n \geq 8760$ thermal cycles/year, then $(\pi_n)_i = 1.7\, n_i^{0.60}$

The temperature acceleration factor is given by the Arrhenius equation, which shows that the rate of change

π_t is a function of the increase in temperature. Each component depends on a specific adjustment value; Table 5 shows the models for each given component.

The reliability standard based on the mission profile is very sensitive to the temperature parameter; this can be seen in Table 5 in the Arrhenius models. Therefore, it is very convenient to define the models to determine the amplitude of the thermal variation for an on/off phase; in the following Table 6, this parameter is defined for each component of the inverter [11, 12, 22].

In the case of low current in the inductor in the on/off phase, $\Delta\tau_i$ is calculated in the same form as in the capacitor. As it has been observed, the thermal effects play a fundamental role in the reliability evaluation. It can be realized that the mission profile is based on the effect of temperature π_t during the performance of photovoltaic systems, as shown by the Arrhenius equation shown in Table 5. It is dependent on the junction temperature in each one of the components that make up the system and the effects $\Delta\tau_i$ of the rate of temperature change during the phases.

The junction temperature T_j for switches and diodes is calculated by (10):

$$T_j = T_C + \left(\theta_{jc}.p_{\text{loss}}\right), \tag{10}$$

where θ_{jc} is the junction-encapsulated thermal resistance, P_{loss} is the losses on the switch, and T_C is the temperature of the package.

The losses in the MOSFET are the sum of static and dynamic losses and are represented by [7, 12, 16, 22]:

$$P_{\text{loss(static)}} = R_{\text{DSon}}.I_{\text{rms}}^2, \tag{11}$$

$$P_{\text{loss(dynamic)}} = V_{\text{avg}}.I_{\text{avg}}.(t_{\text{on}} + t_{\text{off}}).f_{\text{SW}}, \tag{12}$$

$$P_{\text{loss}} = P_{\text{loss(static)}} + P_{\text{loss(dynamic)}}, \tag{13}$$

where P_{loss} is the total power losses, R_{DSon} is the internal resistance, I_{rms} is the effective current, I_{avg} and V_{avg} are the average values, $t_{\text{on}} + t_{\text{off}}$ represent the on and off time, and f_{sw} is the switching frequency.

The power loss of an inductor is defined by:

$$P_{\text{loss\_inductor}} = P_{\text{core}} + P_{\text{dcr}} + P_{\text{acr}}, \tag{14}$$

where P_{core} is the core loss that can be calculated or provided by the manufacturer, P_{dcr} represents the cable loss caused by the DC resistance, and P_{acr} is defined as the cable loss caused by AC resistance.

For this calculation is used [17, 23]:

$$P_{\text{core(mW)}} = K_1 f^x B^y x V_e, \tag{15}$$

where K_1 is the constant for core material, f^x is the frequency in kHz, B^y represents the maximum flux density, x is the frequency exponential function, y is an exponential function of flux density, and V_e is the effective core volume.

Table 5: Arrhenius model.

Component	π_t
Diode	$\pi_t = \exp\left\{4640\left[1/313 - 1/\left(T_j + 273\right)\right]\right\}$
Transistor	$\pi_t = \exp\left\{3480\left[1/373 - 1/\left(T_j + 273\right)\right]\right\}$
Inductor	$\pi_t = \exp\left\{1740\left[1/303 - 1/\left(T_j + 273\right)\right]\right\}$
Capacitor	$\pi_t = \exp\left\{2900\left[1/303 - 1/\left(T_j + 273\right)\right]\right\}$

Table 6: Amplitude of thermal variation in on/off phases.

Component	$\Delta\tau_i$
Diode	$\left[\left(\Delta T_j/3\right) + \left(t_{\text{ac}}\right)_i\right] - \left(t_{\text{ae}}\right)_i$
Transistor	$\left[\left(\Delta T_j/3\right) + \left(t_{\text{ac}}\right)_i\right] - \left(t_{\text{ae}}\right)_i$
Inductor	$\left[\left(\Delta T_R/3\right) + \left(t_{\text{ac}}\right)_i\right] - \left(t_{\text{ae}}\right)_i$
Capacitor	$\left(t_{\text{ac}}\right)_i - \left(t_{\text{ae}}\right)_i$

$$P_{\text{dcr(W)}} = I_{\text{rms}}^2 \text{DCR}, \tag{16}$$

where I_{rms} is the effective value of the peak current applied to the inductor and DCR is the DC resistance of the inductor.

$$P_{\text{acr(W)}} = I_{\text{rms}}^2 \text{ACR}, \tag{17}$$

where I_{rms} represents the effective value of the peak-to-peak ripple current applied to the inductor and ACR is the AC resistance of the inductor.

3. Power Stage and Converter Design

The photovoltaic system is comprised of a photovoltaic panel, a conversion stage, that is the inverter, and the filtering stage.

The stage responsible to inject active power into the grid is the inverter. Main transformerless inverter topologies were described in Section 2, which are full-bridge, double buck, H5, HERIC, H6, NPC, and virtual DC bus.

3.1. Power Stage Design. The inverters were designed for a power of 1 kW, and an LCL filter was used in each of the inverters, since it is intended that all the inverters are under the same operating and design conditions to determine the reliability of each one using the IEC TR 62380 standard for the mission profile.

The selection of the LCL filter was based on its advantages such as smaller size, higher efficiency, lower THD percentage, and better reliability than the L and LC filters [16].

The LCL filter design considers the following aspects. In a photovoltaic system, we have the following relationship:

$$V_g = V_{pv} m, \tag{18}$$

where V_g is the voltage of the electrical grid, V_{pv} is the voltage of the photovoltaic panel, and m is the modulation index.

The resonant frequency must be in a range of values between the network frequency and the switching frequency, satisfying:

$$10f_o \leq f_{res} \leq f_{sw}, \tag{19}$$

where f_0 is the frequency of the electrical grid, f_{res} is the resonant frequency, and f_{sw} is the switching frequency.

The LCL filter is the combination of a capacitor C_f in parallel with two coils L_{f1} and L_{f2}; the calculation of L_{f1} is obtained with:

$$L_{f1} = \frac{V_{pv}(1-m)m}{\Delta_{iLf1} f_{sw}}, \tag{20}$$

where Δ_{iLf1} is the inductor current ripple.

The inductor ratio is determined by α. The relation should be between $\alpha \epsilon$ [3, 7]. The relationship of the individual inductances is

$$L_{f1} = \alpha L_{f2}. \tag{21}$$

The filter capacitor is selected according to (22), and it is a function of ω_{res} the resonant frequency (19) [4, 5, 16], [17]:

$$C_f = \frac{L_{f1} + L_{f2}}{L_{f1} L_{f2} \omega_{\text{res}}}. \tag{22}$$

The design parameters of the inverter and the LCL filter were calculated using equations (18)–(22). The results are shown in Table 7.

3.2. Reliability Design. It is important to define the concept of reliability and the average time between failures, used to evaluate the useful life of the inverters. Reliability was defined previously and is represented as $R(t)$:

$$R(t) = 1 - F(t) = \int_0^t f(t)dt, \tag{23}$$

where $f(t)$ is a function of failure density, t is the time when the component will fail, and $F(t)$ is the cumulative distribution function.

In electronic systems, the exponential distribution is used, giving that represents the useful life of electronic systems with a constant failure rate $\lambda(t)$ assuming that they have survived the initial time. The exponential distribution function is represented by:

$$f(t) = \lambda e^{-\lambda t}. \tag{24}$$

Substituting (24) in (23) and integrating, the exponential reliability function is obtained:

Table 7: Design parameters.

LCL filter
$P_0 = 1\,\text{kW}$
$V_g = 127\,\text{Vrms}$
$V_{pv} = 200\,\text{V}$
$L_{f1} = 425\,\mu\text{H}$
$L_{f2} = 141\,\mu\text{H}$
$C_f = 6.6\,\mu\text{F}$

$$R(t) = e^{-\lambda t}. \tag{25}$$

The average value of the useful life cycle before a failure occurs in the same equipment or component is known as the Mean Time Between Failures (MTBF) and is represented by:

$$\text{MTBF} = \int_0^\infty t f(t)dt = \int_0^\infty \lambda e^{-\lambda t} = \frac{1}{\lambda} = \frac{1}{n\lambda_i}. \tag{26}$$

It is worth mentioning that the reliability with this standard is evaluated in terms of MTBF or FIT (Failures in Time). One FIT equals a one failure in $10E^{9\ \text{hours}}$ [12, 16, 24].

A high number for the MTBF represent good reliability. Once these two concepts have been defined, a reliability analysis is made for each inverter using a serial model. It is known that a system is a grouping of interconnected components. In this way, the reliability of the system will depend on the individual reliability of the components. The serial model is used since in this model if there is a failure in any of the elements or components, the failure of the entire system would be assumed. The serial system is defined as the product of all the individual reliabilities that make up the system. The analysis of $\lambda(t)$ and the MTBF allows determining which component is the weakest. Thus, improving the reliability of this component, the complete system reliability improves.

As an example of calculation, the dual buck inverter (Figure 8) is analyzed using the serial system to determine its reliability.

The following considerations are taken into account for this analysis: the reliability of the switches is equal $R_{S1}(t) = R_{S2}(t) = R_{S3}(t) = R_{S4}(t) = R_1(t)$ and that they present a constant failure rate $\lambda_{S1} = \lambda_{S2} = \lambda_{S3} = \lambda_{S4} = \lambda_1$.

For the diodes, the reliability is considered in a similar manner since they have the same characteristics. Therefore, diodes have a reliability $R_{D1}(t) = R_{D2}(t) = R_{D3}(t) = R_{D4}(t) = R_2(t)$ and a constant failure rate $\lambda_{D1} = \lambda_{D2} = \lambda_{D3} = \lambda_{D4} = \lambda_2$.

In the case of the inductors and the filter capacitor, the reliability is as follows. For the inductor L_{f1}, there is a reliability $R_{Lf1}(t) = R_3(t)$ and a failure rate $\lambda_{Lf1} = \lambda_3$. The capacitor C_f has a reliability $R_{Cf}(t) = R_4(t)$ and a failure rate $\lambda_{Cf} = \lambda_4$. Finally, the inductor L_{f2} presents a reliability $R_{Lf2}(t) = R_5(t)$ and a failure rate $\lambda_{Lf2} = \lambda_5$.

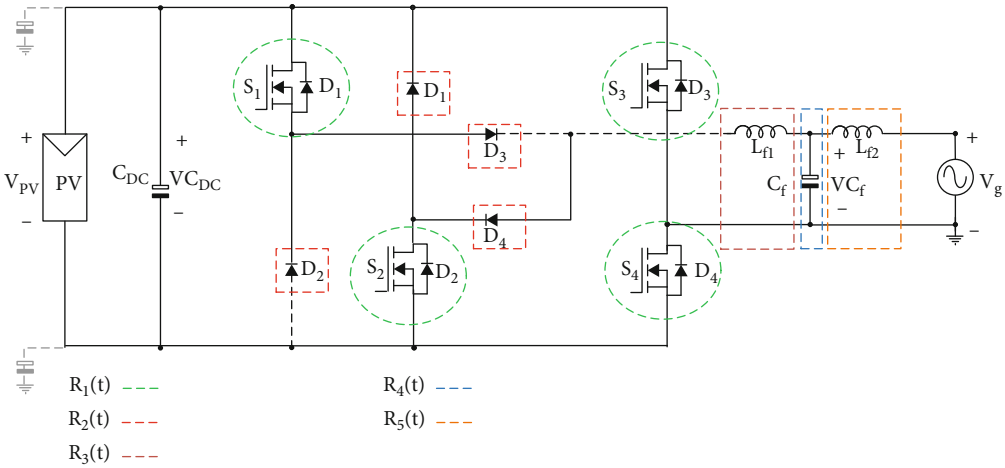

Figure 8: Serial analysis of the double buck inverter.

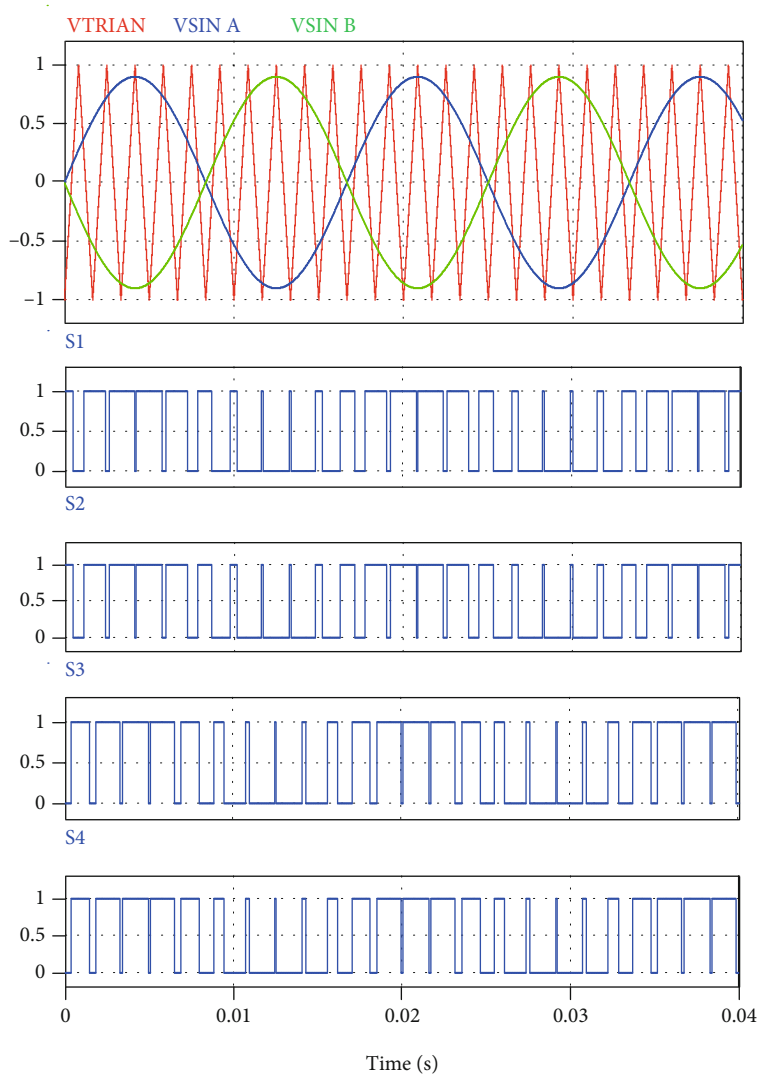

Figure 9: Unipolar modulation and control signals. (a–e) Modulation signals (0.5 V/div) and control signals (1 V/div).

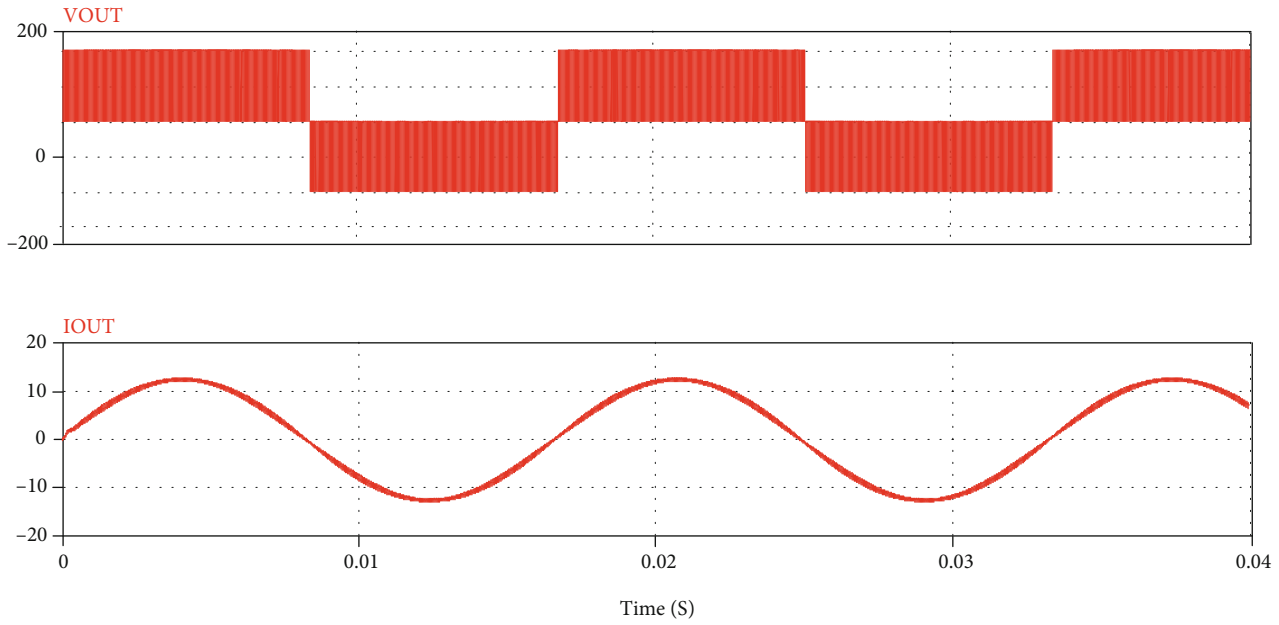

Figure 10: Inverter output voltage before filter. (a, b) Output voltage (100 V/div) and output current (10 A/div).

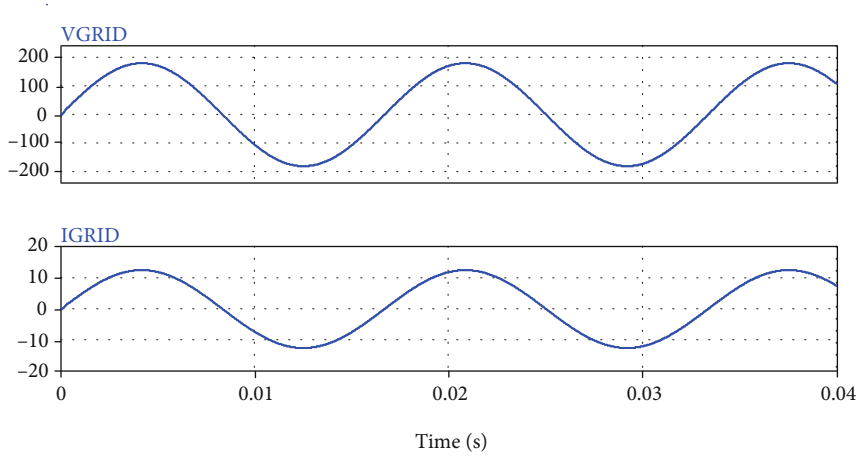

Figure 11: Active power injection to the grid. (a, b) Filter output voltage (100 V/div) and filter output current (10 A/div).

Solving the serial system would be as follows:

$$R_S(t) = R_1(t).R_2(t).R_3(t).R_4(t).R_5(t). \quad (27)$$

Substituting the exponential reliability function (25) in (27), the reliability of the series system is

$$R_S(t) = e^{-(4\lambda_1+4\lambda_2+\lambda_3+\lambda_4+\lambda_5)t}. \quad (28)$$

The MTBF is calculated by substituting (28) in (26), where the following relationship is obtained:

$$\text{MTBF} = \frac{1}{4\lambda_1 + 4\lambda_2 + \lambda_3 + \lambda_4 + \lambda_5}. \quad (29)$$

The process described above is made for each of the inverters described.

4. Simulation and Reliability Results

The simulation of the inverters was carried out using the PSIM® software, as it is a very versatile software that allows fast simulation, thanks to the wide variety of device models it handles.

The simulation of each of the inverters was carried out using a unipolar open-loop modulation, since it is the type of modulation that the branches switch at high frequency, allowing the output filter to be small and having high efficiency, in addition to generating three voltage levels at the output.

In the filtering and coupling stage, the LCL filter will be used for all cases. SiC MOSFETs are used in the simulation, C3M0065090D (CREE Manufacturer). Considering the parameters according to the manufacturer's data sheet and a behavior similar to the real environment as required by

the standard, the simulations were made. For this analysis, a test ambient temperature provided by the mission profile was used, which is at which the device operates during the mission profile [16].

The simulation is performed to obtain operating parameters required for the calculation of reliability, such as voltages and currents. The failure rate adjustment models require nominal, average, or effective values for each device. In the case of the load factor, it requires maximum operating values. In the case of the temperature factor, it depends on the junction temperature of the device; therefore, average and effective values are used.

4.1. Simulation Results. The simulation results in PSIM® are shown in Figures 9–11. The control signals obtained are consistent for a unipolar modulation; for illustrating purposes in Figure 9, a switching frequency lower than the used was graphed to make it visible. Unipolar modulation signals can be observed from top to bottom on a 0.5 V/div scale and the control signals S_1, S_2, S_3, and S_4 on a 0.5 V/div scale.

In Figure 10, it can be seen from top to bottom the output voltage of the inverter before the output filter on a scale of 100 V/div and the current of 8.3 A at a scale of 10 A/div.

In Figure 11, it is observed from top to bottom the output voltage of the inverter after the filter, where a power of 1 kW would be injected into the grid. A voltage of 180 V is observed on a scale of 100 V/div and a current of 8.3 A at a scale of 10 A/div.

In Table 8, an inverter comparative analysis of the semiconductor elements is shown, as well as their efficiency, which is a parameter on which reliability depends. The efficiency of the inverters was obtained based on the simulation with a unipolar modulation for each case.

Another important parameter by which reliability is also measured is THD percentage. These parameters are directly related since they are attributes that allow evaluating the quality of the system. THD directly affects inverter reliability; it is related to the quality and safety of the system. The term quality refers mainly to the quality of the signal wave and safety; it is related to the system complying with the THD limits allowed by regulations. Table 9 shows the THD percentage of the analyzed inverters, as well as the switches that switch at high or low frequency.

Tables 8 and 9 show that comparing single-phase inverters, the one with the best characteristics in both efficiency and THD is the full-bridge inverter, with an efficiency of 99.05% and a THD of 0.08200899%, followed by the virtual DC bus with 99.00% efficiency and a THD of 0.01021878%, and double buck with 98.93% efficiency and THD of 0.08270188%.

4.2. Reliability Calculation Results. The numerical reliability calculation is performed using the IEC TR 62380 standard. Table 10 shows the base factors taken from the standard for each of the components that make up the inverters. The λ_B corresponds to the TO-220 package. The λ_{EOS} factor corresponds to the type of telecommunication mission profile.

Table 11 shows the mission profile, which complies with the total annual relationship of times given in equation (3).

Table 8: Comparison of number of elements and inverter efficiency.

Topology	Switches	Diodes	Capacitors	Efficiency
Full bridge	4	X	X	99.05%
Double buck	4	4	X	98.93%
H5	5	X	X	98.67%
HERIC	6	X	X	98.53%
H6	6	2	X	98.55%
NPC	4	2	X	98.86%
Virtual DC bus	5	X	1	99.00%

X indicates that it is not applied for the system.

Table 9: Inverter THD comparison.

Topology	High frequency	Low frequency	%THD
Full bridge	S_1, S_2, S_3, S_4	X	0.08200899
Double buck	S_1, S_2, S_3, S_4	X	0.08270188
H5	S_2, S_4, S_5	S_1, S_3	0.22131262
HERIC	S_1, S_2, S_3, S_2	S_5, S_6	0.22176104
H6	S_1, S_2, S_5, S_6	S_3, S_4	0.22176183
NPC	S_1, S_4	S_2, S_3	0.17539819
Virtual DC bus	S_1, S_2, S_3, S_4, S_5	X	0.01021878

X indicates that it is not applied for the system.

Table 10: Adjustment factors for power components.

Component	λ_0	λ_B	λ_{EOS}	π_U	π_1
Diode	0.7 FIT	5.7	40	1	1
Transistor	2 FIT	5.7	40		1
Inductor	0.6 FIT				

There is only one annual working phase to consider for a permanent working.

The mission profile of Table 11 is given for a permanent working; inverters operate with conditions, and values for "ground; stationary; non weather protected"(ground; fixed for Mil-HDBK-217F) can be calculated for various climates.

The mission profile is related to the failure rate adjustment equations shown in Tables 1–4. The time parameters and operating cycles shown in Table 11 are applied to the adjustment equations. The temperature factor is determined by the temperature of Table 11, and the junction temperature is obtained with values from simulation, using the Arrhenius model.

Table 12 shows the results of the reliability calculations for each of the single-phase inverters analyzed in this study. It can be observed that the full-bridge inverter and virtual DC bus present better reliability compared to the other inverters, with a lower failure rate and a higher MTBF.

The full-bridge being the best of these, with a 193.415FIT failure rate and an MTBF of 0.005171FIT, followed by the virtual DC bus with a 240.671FIT failure rate and

Table 11: Mission profile.

Application type	Environment type	Equipment type	$(t_{ae})i$ °C	$(t_{ac})_i$ °C	τ_1	τ_{on}	T_{off}	n_1 cycles/year	ΔT_1 °C/cycle
Telecom	Ground fixed (GF)	Transmitting and access	11	31	0.5	0.25	0.25	365	8

Table 12: Total reliability of inverters.

Topology	$\lambda_{System(FIT)}$	MTBF (FIT)
Full bridge	193.415	0.005171
Double buck	377.555	0.002649
H5	332.691	0.003006
HERIC	379.937	0.002632
H6	379.997	0.002632
NPC	285.485	0.003503
Virtual DC bus	240.671	0.004155

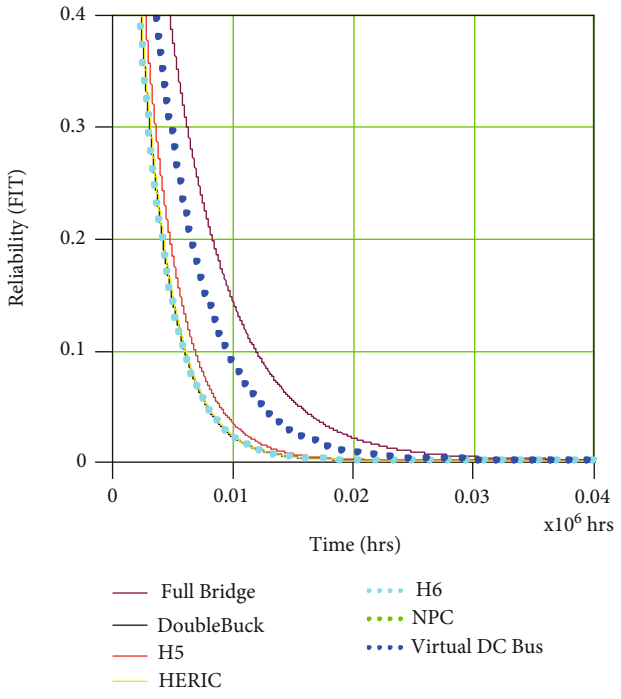

Figure 12: Comparative graph of the reliability of single-phase inverters.

0.004155FIT MTBF. The virtual DC bus inverter and the HERIC present a very similar failure rate and MTBF, only differentiated by the contribution of some element's failure rate in the NPC inverter. The inverters with the worst reliability are the HERIC with a failure rate of 379.937FIT and a 0.002632FIT MTBF and the H6 with a 379.997FIT failure rate and a 0.002632FIT MTBF.

In Figure 12, a comparative graph of the reliability of the different single-phase inverters analyzed is observed, represented in FIT. Analyzing the best case of the full-bridge inverter, it has an MTBF of 0.005171FIT, equivalent to an annual failure probability of 0.16% and reliability of

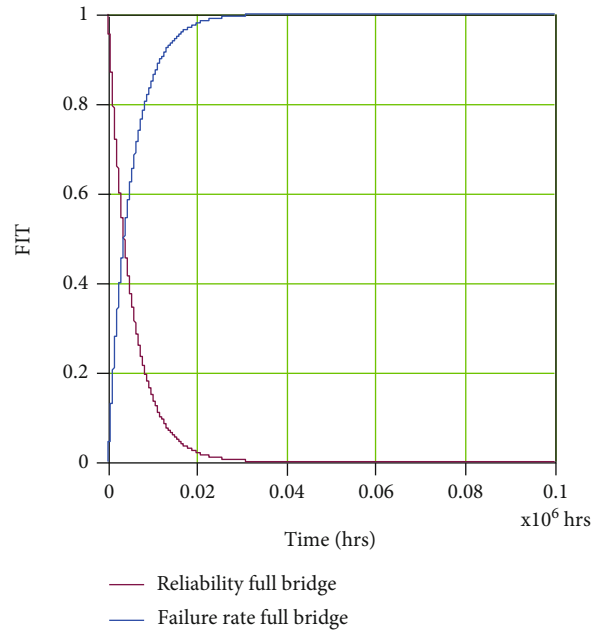

Figure 13: Representation of the probability of failure of the full-bridge inverter.

98.40%. Now the worst case, the H6 inverter has an MTBF of 0.002632FIT, equivalent to an annual failure probability of 0.33% and reliability of 96.70%. The number of years also indicates that the inverter that would present a probability of failure in the first instance is the H6. It can be seen that the curve of the complete bridge has a longer lifetime compared to the other inverters. The full-bridge turned out to be the most reliable inverter; it is convenient to represent the reliability cumulative distribution function (24). The cumulative distribution function can be interpreted as the probability of failure presented by the system in FIT. In Figure 13, a relationship between the reliability function and the failure probability function of the full-bridge inverter is observed, through an equilibrium point at the intersection of the curves.

It is important to highlight, although the full-bridge inverter has better reliability and efficiency, its use is not recommended; since it presents a leakage current between the PV and ground, and it is higher than that allowed by the European standard VDE 0126-1-1 [25], which should not be higher than 300 mA.

Table 13 shows the percentage of contribution of each component to the total failure rate of the system, concerning the number of components in Table 8. It is observed that the failure rate depends directly on the number of components that make up the system. Therefore, the reliability is directly related to the number of elements that the system has. In

Table 13: Percentage of contribution to the failure rate of the photovoltaic system.

Topology	Inverter failure rate				LCL filter failure rate	
	Switches		Diodes	Capacitors	Inductors	Capacitors
	MOSFET	Parasitic diode				
Full bridge	97.73%	X	X	X	2.21%	0.06%
Double buck	50.06%	X	48.77%	X	1.13%	0.04%
H5	71.00%	27.67%	X	X	1.30%	0.03%
HERIC	74.61%	24.23%	X	X	1.13%	0.03%
H6	74.61%	X	24.22%	X	1.13%	0.04%
NPC	66.21%	X	32.25%	X	1.51%	0.03%
Virtual DC bus	98.14%	X	X	0.04%	1.78%	0.04%

X indicates that it is not applied for the system.

addition, it is visible that in each one of the inverters that were analyzed, which are the components that have the most contribution to the failure rate of the system, that is, the components that may have the most failures and that may have a shorter lifetime. To reduce the power losses and increase reliability, the C3M0065090D SiC MOSFET (CREE Manufacturer) is used. Since the turn-on resistance is too low, a synchronous rectification occurs when the current becomes negative in the device; therefore, the free-wheeling diode does not conduct during this time, as traditionally occurs in the inverters. Since the MOSFET's voltage drop is smaller than the diode forward voltage, the MOSFET conducts for positive and negative currents, Certainly, there are some topologies where diodes conduct and synchronous rectification does not occur.

In general, in inverters, the highest percentage of failure contribution is made by the switches, followed by the diodes, then the inductors, and with the lowest percentage the capacitors. The characteristics of an MKP capacitor were used; it has advantages such as thermal and electrical stability, reliability, and a long useful life.

It is also observed that the switching frequency is a parameter that greatly affects the reliability. If the switching frequency is reduced, the reduction of losses is considerable. When determining reliability, the parameter that is related to the standard, through the Arrhenius model, is the junction temperature and thermal resistance of the component encapsulation. Therefore, the failure rate depends on the bonding temperature and the temperature in the casing; this is on the mission temperature profile. Reducing the switching frequency reduces the component failure rate by 0.10%. Then, it is obtained a λ_{system} = 193.214FIT and an increment of the MTBF to 0.005176FIT.

Other simulations were carried out to verify the impact of the device on the reliability; a 3rd Generation SiC MOSFET (C3M0025065D) was used since the internal resistance is smaller, as mentioned previously. Then, better results were obtained; the losses were reduced, and there is a positive, but small, effect on reliability.

Following the analysis that has been made is recommended to the designer to increase the MTBF of the systems, since it is the parameter that measures the useful life of the system. This may be achieved by using component heat dissipation and cooling systems to reduce thermal stress and at the same time reduce the component failure rate as well as using devices made of better materials such as silicon carbide, which have lower (better) thermal resistance.

Also, from the analysis, the converter with fewer components will be the best option for reliability but not forgetting the leakage current of the PV system. Then, of all the inverters studied, the best alternative is the virtual DC bus inverter with SiC devices. This is because it offers a low THD, high efficiency, best reliability, and useful life while satisfying the leakage currents for PV system standards. The following alternative is the NPC inverter. Certainly, the final selection of the inverter is left to the designer, since the difference is relatively small between them.

5. Conclusion

This article presents the prediction of the reliability of different single-phase inverters using an LCL filter in the filtering stage. For the calculation and approximation of the prediction of the reliability, the standard IEC TR 62380 is used.

In this study, they were compared the full-bridge, double buck, H5, HERIC, H6, NPC, and virtual DC bus converters. The full-bridge inverter presents better reliability and better useful life. In addition, it features a higher THD percentage, at better efficiency. The virtual DC bus and NPC inverters have the following best realiability, there is a small difference in reliability and efficiency. The use of a virtual DC bus inverter with SiC devices is recommended since the full-bridge presents higher leakage current than allowed by the standards.

The study shows that the devices present a failure rate percentage in the following order: switches, diodes, inductors, and to a lesser extent, capacitors. It was observed that the switching frequency affects the reliability of the component to a lesser extent.

The parameter that directly affects reliability is the number of elements that make up the system. The reliability and average useful life of the systems can be increased, using cooling systems to reduce thermal stress, which is the parameter that directly relates to the failure rate and therefore the reliability of the system. It is also recommended to use silicon carbide devices, which are components with smaller internal resistance and thermal resistance that allows to have few losses, high efficiency, and reliability.

Data Availability

All the data used is in the paper.

Conflicts of Interest

The authors declare that there is no conflict of interest regarding the publication of this paper.

Acknowledgments

This work was supported in part by the TecNM under project no. 13133.21-P and by the SENACyT under project no. ITE17-R2-006.

References

[1] N. L. Panwar, S. C. Kaushik, and S. Kothari, "Role of renewable energy sources in environmental protection: a review," *Renewable and Sustainable Energy Reviews*, vol. 15, no. 3, pp. 1513–1524, 2011.

[2] M. D. Leonard, E. E. Michaelides, and D. N. Michaelides, "Energy storage needs for the substitution of fossil fuel power plants with renewables," *Renewable Energy*, vol. 145, pp. 951–962, 2020.

[3] M. A. Basit, S. Dilshad, R. Badar, and S. M. Sami ur Rehman, "Limitations, challenges, and solution approaches in grid-connected renewable energy systems," *International Journal of Energy Research*, vol. 44, no. 6, pp. 4132–4162, 2020.

[4] W. Li, Y. Gu, H. Luo, W. Cui, X. He, and C. Xia, "Topology review and derivation methodology of single-phase transformerless photovoltaic inverters for leakage current suppression," *IEEE Transactions on Industrial Electronics*, vol. 62, no. 7, pp. 4537–4551, 2015.

[5] L. S. Xavier, A. F. Cupertino, H. A. Pereira, and V. F. Mendes, "Partial harmonic current compensation for multifunctional photovoltaic inverters," *IEEE Transactions on Power Electronics*, vol. 34, no. 12, pp. 11868–11879, 2019.

[6] K. Zeb, W. Uddin, M. A. Khan et al., "A comprehensive review on inverter topologies and control strategies for grid connected photovoltaic system," *Renewable and Sustainable Energy Reviews*, vol. 94, pp. 1120–1141, 2018.

[7] M. H. Ahmed, M. Wang, M. A. S. Hassan, and I. Ullah, "Power loss model and efficiency analysis of three-phase inverter based on SiC MOSFETs for PV applications," *IEEE Access*, vol. 7, pp. 75768–75781, 2019.

[8] M. C. Cavalcanti, A. M. Farias, K. C. Oliveira, F. A. S. Neves, and J. L. Afonso, "Eliminating leakage currents in neutral point clamped inverters for photovoltaic systems," *IEEE Transactions on Industrial Electronics*, vol. 59, no. 1, pp. 435–443, 2012.

[9] Y. Yang, K. Ma, H. Wang, and F. Blaabjerg, "Mission profile translation to capacitor stresses in grid-connected photovoltaic systems," in *2014 IEEE Energy Conversion Congress and Exposition (ECCE)*, pp. 5479–5486, Pittsburgh, PA, USA, 2014.

[10] A. Sangwongwanich, Y. Yang, D. Sera, and F. Blaabjerg, "Mission profile-oriented control for reliability and lifetime of photovoltaic inverters," *IEEE Transactions on Industry Applications*, vol. 56, no. 1, pp. 601–610, 2020.

[11] "A Universal Model for Reliability Prediction of Electronics Components, PCBs and Equipment," in *Reliability Data Handbook*, Union Technique de L'Electricite, UTE C 80-810, 1st ed edition, 2000.

[12] S. E. De León-Aldaco, H. Calleja, F. Chan, and H. R. Jiménez-Grajales, "Effect of the mission profile on the reliability of a power converter aimed at photovoltaic applications-a case study," *IEEE Transactions on Power Electronics*, vol. 28, no. 6, pp. 2998–3007, 2013.

[13] N. Sintamarean, F. Blaabjerg, H. Wang, and Y. Yang, "Real field mission profile oriented design of a SiC-based PV-inverter application," *IEEE Transactions on Industry Applications*, vol. 50, no. 6, pp. 4082–4089, 2014.

[14] Y. Yang, H. Wang, and F. Blaabjerg, "Reliability assessment of transformerless PV inverters considering mission profiles," *International Journal of Photoenergy*, vol. 2015, Article ID 968269, 10 pages, 2015.

[15] M. Shayestegan, M. Shakeri, H. Abunima et al., "An overview on prospects of new generation single-phase transformerless inverters for grid-connected photovoltaic (PV) systems," *Renewable and Sustainable Energy Reviews*, vol. 82, pp. 515–530, 2018.

[16] I. Villanueva, N. Vázquez, J. Vaquero, C. Hernández, H. López, and R. Osorio, "L vs. LCL filter for photovoltaic grid-connected inverter: a reliability study," *International Journal of Photoenergy*, vol. 2020, Article ID 7872916, 10 pages, 2020.

[17] P. Channegowda and V. John, "Filter optimization for grid interactive voltage source inverters," *IEEE Transactions on Industrial Electronics*, vol. 57, no. 12, pp. 4106–4114, 2010.

[18] N. Vázquez, M. Rosas, C. Hernández, E. Vázquez, and F. J. Perez-Pinal, "A new common-mode transformerless photovoltaic inverter," *IEEE Transactions on Industrial Electronics*, vol. 62, no. 10, pp. 6381–6391, 2015.

[19] S. V. Araujo, P. Zacharias, and R. Mallwitz, "Highly efficient single-phase transformerless inverters for grid-connected photovoltaic systems," *IEEE Transactions on Industrial Electronics*, vol. 57, no. 9, pp. 3118–3128, 2010.

[20] L. Zhou and F. Gao, "Dual buck inverter with series connected diodes and single inductor," in *2016 IEEE Applied Power Electronics Conference and Exposition (APEC)*, pp. 2259–2263, Beach, CA, USA, 2016.

[21] "Reliability Methodology for Electronic Systems," in *FIDES guide 2009 Edition A*, FIDES group, 2010.

[22] "Universal Model for Reliability Prediction of Electronic Components, PCBs and Equipment," in *Reliability Data Handbook*, Technical Report IEC TR 62380, 1st ed edition, 2004.

[23] Y. Zhou, W. Huang, F. Hong, and C. Wang, "Modelling analysis and power loss of coupled-inductor single-stage boost inverter based grid-connected photovoltaic power system," *IET Power Electronics*, vol. 9, no. 8, pp. 1664–1674, 2016.

[24] F. Richardeau and T. T. L. Pham, "Reliability calculation of multilevel converters: theory and applications," *IEEE Transactions on Industrial Electronics*, vol. 60, no. 10, pp. 4225–4233, 2013.

[25] X. Guo, N. Wang, J. Zhang, B. Wang, and M. K. Nguyen, "A novel transformerless current source inverter for leakage current reduction," *IEEE Access*, vol. 7, pp. 50681–50690, 2019.